JACS
JOURNAL OF THE AMERICAN CHEMICAL SOCIETY
pubs.acs.org/JACS
Article

Stereoelectronic Effects Impact Glycan Recognition

Caitlin M. McMahon,[§] Christine R. Isabella,[§] Ian W. Windsor, Paul Kosma, Ronald T. Raines, and Laura L. Kiessling*

Cite This: J. Am. Chem. Soc. 2020, 142, 2386−2395
Read Online
ACCESS | Metrics & More | Article Recommendations | Supporting Information

ABSTRACT: Recognition of distinct glycans is central to biology, and lectins mediate this function. Lectin glycan preferences are usually centered on specific monosaccharides. In contrast, human intelectin-1 (hItln-1, also known as Omentin-1) is a soluble lectin that binds a range of microbial sugars, including β-D-galactofuranose (β-Galf), D-glycerol 1-phosphate, D-*glycero*-D-*talo*-oct-2-ulosonic acid (KO), and 3-deoxy-D-*manno*-oct-2-ulosonic acid (KDO). Though these saccharides differ dramatically in structure, they share a common feature—an exocyclic vicinal diol. How and whether such a small fragment is sufficient for recognition was unclear. We tested several glycans with this epitope and found that L-*glycero*-α-D-*manno*-heptose and D-*glycero*-α-D-*manno*-heptose possess the critical diol motif yet bind weakly. To better understand hItln-1 recognition, we determined the structure of the hItln-1·KO complex using X-ray crystallography, and our 1.59 Å resolution structure enabled unambiguous assignment of the bound KO conformation. This carbohydrate conformation was present in >97% of the KDO/KO structures in the Protein Data Bank. Bioinformatic analysis revealed that KO and KDO adopt a common conformation, while heptoses prefer different conformers. The preferred conformers of KO and KDO favor hItln-1 engagement, but those of the heptoses do not. Natural bond orbital (NBO) calculations suggest these observed conformations, including the side chain orientations, are stabilized by not only steric but also stereoelectronic effects. Thus, our data highlight a role for stereoelectronic effects in dictating the specificity of glycan recognition by proteins. Finally, our finding that hItln-1 avoids binding prevalent glycans with a terminal 1,2-diol (e.g., *N*-acetyl-neuraminic acid and L-*glycero*-α-D-*manno*-heptose) suggests the lectin has evolved to recognize distinct bacterial species.

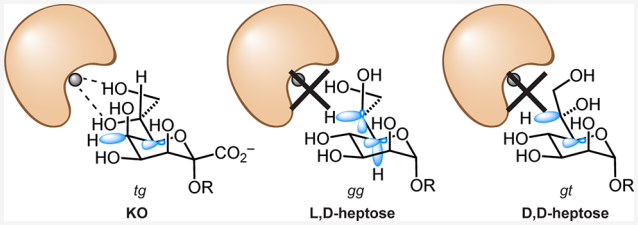

INTRODUCTION

Lectins can selectively target specific cell types by recognizing cell-surface glycans. In this way, lectins mediate diverse processes ranging from fertilization to pathogen clearance and the immune response.[1−4] An understanding of the molecular basis for glycan recognition is critical for determining lectin selectivity and therefore lectin function. Lectin−carbohydrate specificity can be elucidated using a combination of glycan-array profiling, nuclear magnetic resonance (NMR) spectroscopy, carbohydrate modeling, computational studies, bioinformatics, and X-ray crystallography.[5−9] Still, glycan recognition specificity is difficult to predict.

Hydrogen bonding with sugar hydroxyl groups, CH−π interactions with aromatic amino acid side chains, and coordination to calcium ions can contribute to carbohydrate binding (Figure 1a).[5,7,10−13] Although carbohydrates are often considered to be flexible, influences such as steric repulsion, torsional strain, and stereoelectronic effects can give rise to conformational preferences.[14,15] Individual saccharide binding constants are relatively weak because the glycan binding sites of lectins are not deep clefts but rather solvent exposed. As a result, the low-energy saccharide conformations, most commonly discussed in terms of φ, ψ, and ω dihedral angles (Figure 1c),[16] are those typically recognized and bound by proteins.[17,18] Most studies conducted to date have focused on the recognition of hexoses in the pyranose form, as these are common building blocks of mammalian glycans. Much less is known about how lectins recognize microbial saccharides, which include furanose sugars, the ulosonic acids (D-*glycero*-D-*talo*-oct-2-ulosonic acid (KO), 3-deoxy-D-*manno*-oct-2-ulosonic acid (KDO)), and the heptoses (L-*glycero*-α-D-*manno*-heptose and D-*glycero*-α-D-*manno*-heptose). Our studies of human intelectin-1 (hItln-1), a soluble lectin that recognizes specifically the glycan residues found on microbial cells, prompted us to explore the conformations of these bacterial saccharides.

HItln-1 is expressed at mucosal barriers in the small intestine and the lung,[19−21] and has been implicated in diseases associated with dysbiosis of the microbiome, including Crohn's disease, ulcerative colitis, asthma, and diabetes.[22−24] We found that hItln-1 is a trimeric protein that binds the microbial

Received: October 30, 2019
Published: January 13, 2020

https://dx.doi.org/10.1021/jacs.9b11699
J. Am. Chem. Soc. 2020, 142, 2386−2395

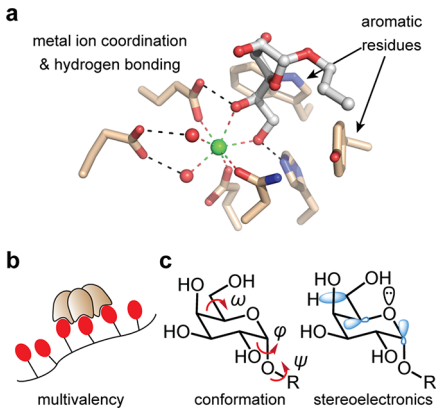

Figure 1. Factors contributing to lectin−carbohydrate binding and recognition. (a) The binding site of the complex of hItln-1 and allyl-*β*-Gal*f* is depicted with hydrogen bonding and metal ion coordination with the hydroxyl groups of sugars represented. Aromatic residues play crucial roles in many sugar−protein complexes. (b) Human Itln-1 is a trimer, which can engage in multivalent binding to glycan-displaying surfaces or proteins. (c) Carbohydrate conformations are characterized by three dihedral angles (*φ*, *ψ*, *ω*). Flexibility at these positions results in multiple conformational possibilities, influencing overall shape and recognition. Stereoelectronic effects influence the prevalence of distinct sugar conformations.

monosaccharide *β*-D-galactofuranose (*β*-D-Gal*f*) through the Ca^{2+}-coordination of its exocyclic vicinal diol (Figure 1a).[25] This epitope proved to be a determining feature for binding, as a glycan array revealed hItln-1 preferentially bound to polysaccharides containing residues with an exocyclic vicinal diol (e.g., *β*-Gal*f*, glycerol 1-phosphate) over those without it. Moreover, the diol-recognition motif is conserved across species as the frog intelectin, XEEL, interacts with glycerol-1-phosphate through a similar binding mode.[26] Still, hItln-1 does not bind all sugars with this epitope, as sialic acid, which is a common mammalian sugar, possesses such a diol but is not a ligand for hItln-1.[25] These data indicate there are other determinants of recognition.

We investigated the binding of hItln-1 to saccharide residues that possess a terminal 1,2-diol, including KO, KDO, L-*glycero*-*α*-D-*manno*-heptose (L,D-heptose), and D-*glycero*-*α*-D-*manno*-heptose (D,D-heptose).[25] These sugars are present in bacterial lipopolysaccharide (LPS) structures that can stimulate innate immunity, and all feature an exocyclic vicinal diol that could facilitate recognition by hItln-1.[27] Our data reveal that these saccharides have conformational preferences that maximize favorable stereoelectronic effects and, in turn, dictate their ability to bind lectins. These findings provide guidelines for predicting the bound conformation of bacterial sugars.[28] Because small differences in monovalent protein−carbohydrate interactions are amplified through multivalency,[29,30] the conformational differences we observed can make critical contributions to lectin recognition and specificity.

RESULTS

hItln-1 Binding to Microbial Monosaccharides. Our previous microbial glycan array profiling identified several putative monosaccharide ligands of hItln-1, including glycerol 1-phosphate, KO, KDO, and L,D-heptose. Each of these saccharides has an exocyclic vicinal diol, the required epitope for calcium ion coordination in the hItln-1 binding site, but

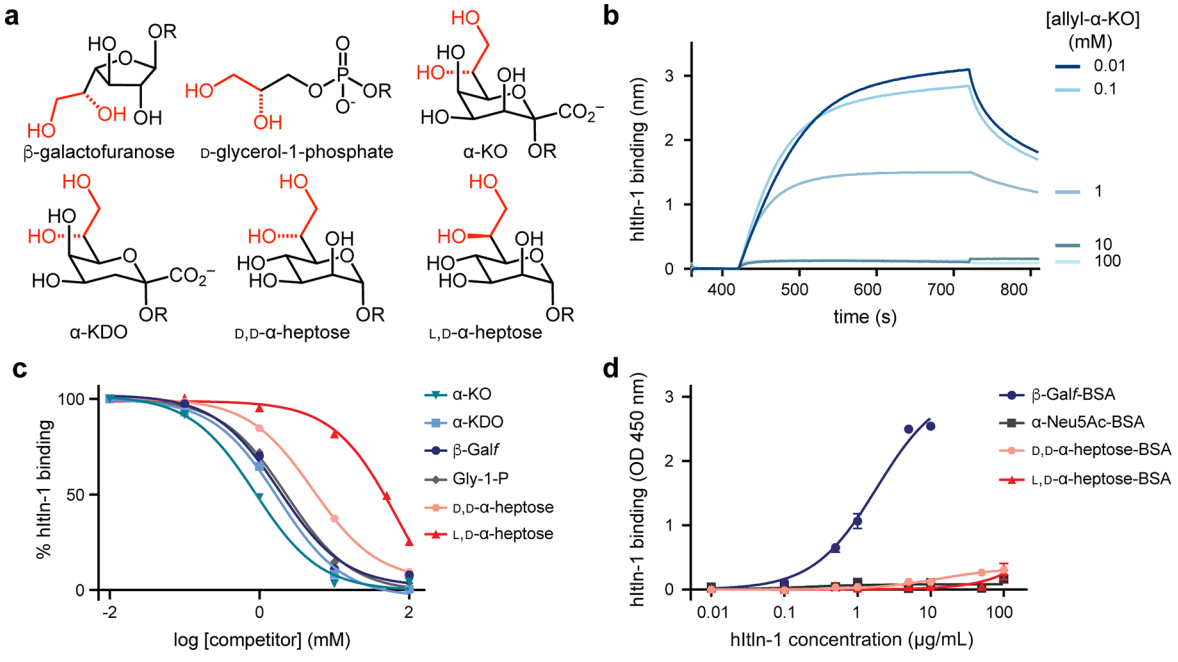

Figure 2. Human intelectin-1 (hItln-1) binding to monosaccharides. (a) Structures of monosaccharides identified as potential hItln-1 ligands from glycan microarray and evaluated in hItln-1 binding studies. (b) Representative real-time biolayer interferometry sensorgram (BLItz) of competition of hItln-1 binding to immobilized biotinylated Gal*f* with varying concentrations of soluble allyl-*α*-D-*glycero*-D-*talo*-oct-2-ulosonic acid (allyl-*α*-KO). (c) Competition of soluble monosaccharide epitopes with immobilized *β*-Gal*f* using BLItz. End point data (710−720 s) from BLItz sensorgrams were averaged and normalized for each competitor concentration and fitted to a one site log IC_{50} equation (solid lines). IC_{50} values were determined (Table 1). The allyl glycoside of each compound in the anomer shown in (a) was tested in the competition assay. (d) Evaluation of BSA-conjugated heptose sugars as ligands for hItln-1 using ELISA. Data shown as mean ± SEM (n = 2 technical replicates). Data were fitted to a single-site binding equation (solid lines). K_d values could not be determined for L,D-heptose or D,D-heptose. OD, optical density.

https://dx.doi.org/10.1021/jacs.9b11699
J. Am. Chem. Soc. 2020, 142, 2386−2395

Table 1. IC_{50} Values of Ligands and Corresponding Changes in Free Energy of Binding Compared to KO

	KO	KDO	Gal*f*	glycerol 1-phosphate	D,D-heptose	L,D-heptose
IC_{50} (mM)[a]	0.7 (±0.3)	1.5 (±0.4)	1.8 (±0.1)	2.1 (±0.4)	6.8 (±2.3)	53 (±29)
ΔΔ*G*(kcal/mol)[b]						
KO	–	–	–	–	–	–
KDO	0.4	–	–	–	–	–
β-Gal*f*	0.6	0.1	–	–	–	–
glycerol 1-phosphate	0.7	0.2	0.1	–	–	–
D,D-heptose	1.3	0.9	0.8	0.7	–	–
L,D-heptose	2.6	2.0	2.0	1.9	1.2	–

[a]Data is shown as mean (±standard deviation) of two independent experiments. [b]The relative free energy of binding is $\Delta\Delta G = 0.593$ (kcal/mol) $\ln(IC_{50,row}/IC_{50,column})$.

whether all bind hItln-1 was unclear. Specifically, glycan hits containing heptose ligands also had KO and/or KDO residues. We addressed this issue with a competition assay in which soluble monosaccharides were assessed for their ability to compete with hItln-1 binding to immobilized *β*-Gal*f*. Using biolayer interferometry (BLI), we determined the half maximal inhibitory concentrations (IC_{50} values) for *β*-Gal*f*, glycerol 1-phosphate, KO, KDO, and L,D-heptose (Figure 2, Table 1). Allyl-KO was the most effective competitor, followed by allyl-KDO and D-glycerol 1-phosphate. L,D-Heptose was a weaker binder, exhibiting an IC_{50} value 80-fold higher than that of allyl-KO. The IC_{50} values were used to estimate the relative free energy (ΔΔ*G*) of binding between the test ligands, which revealed a 2.6 kcal/mol decrease in binding energy for L,D-heptose versus KO (Table 1). Because the exocyclic vicinal diol is engaged in calcium coordination, we first compared its conformation. The stereochemistry at the C6-position of L,D-heptose differs from that of the corresponding side chain of KO and KDO (C7). We therefore evaluated hItln-1 binding to D,D-heptose, as the diol configuration matches that of KO and KDO. D,D-Heptose is a less naturally abundant microbial monosaccharide than L,D-heptose[31] and was less frequently represented on the glycan array. Competition of D,D-heptose with hItln1-Gal*f* binding afforded an IC_{50} of 6.8 mM, indicating that D,D-heptose is a better ligand than L,D-heptose but not as effective as KO, KDO, or *β*-Gal*f*.

HItln-1 is a trimer; therefore, like many oligomeric lectins, hItln-1 can engage in multivalent interactions at the cell surface. Monovalent carbohydrate ligands tend to bind proteins with low affinities and free energies of binding (i.e., K_d values that are often in the millimolar range), and oligomeric lectins can take advantage of multivalency to achieve functional avidity.[29,32] Differences in monovalent binding affinity are amplified through multivalency to endow glycan-binding proteins with high specificity for cell-surface recognition. We therefore tested the specificity of hItln-1 in an assay that relies on multivalency. Specifically, we conjugated multiple copies of each saccharide tested to bovine serum albumin (BSA), and assessed its ability to bind hItln-1 in an enzyme-linked immunosorbent-like assay (ELISA).[33] We observed the same general trends in monosaccharide binding as in the monovalent assay (Figure 2, Figure S4), but the selectivity in this assay was much higher. We detected no measurable binding to hItln-1 by ELISA for L,D- or D,D-heptose.

Our data indicate KO and KDO, along with *β*-Gal*f* and glycerol 1-phosphate, are the most relevant ligands from the observed glycan array hits. They are bound by hItln-1 with higher affinity than the heptoses. The weaker inhibitory activities of L,D-heptose and D,D-heptose point to the importance of hydroxyl group stereochemistry. We postulated that the effect of stereochemistry arises from stereoelectronic effects that dictate side chain conformation and therefore hItln-1 binding.

Structure of hItln-1 Bound to Allyl-KO. To understand the molecular mechanisms underlying saccharide selectivity by hItln-1, we solved the structure of allyl-*α*-KO bound to hItln-1 by X-ray crystallography (Figure 3, Table S1). As we reported

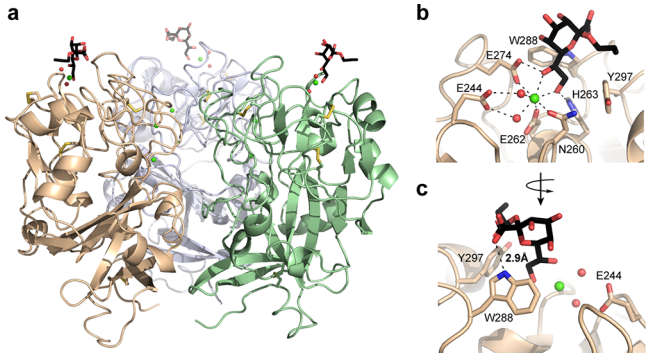

Figure 3. Structure of hItln-1 bound to allyl-*α*-KO. (a) Complex of hItln-1 trimer and allyl-*α*-KO. The lectin monomers are depicted in green, wheat, or light blue; the allyl-*α*-KO in black; calcium ions in green; intramonomer disulfides in yellow; and ordered water molecules in the binding site in red. The trimeric structure is produced from chain A in the asymmetric unit by a three-fold crystallographic operation. (b) The carbohydrate-binding site of hItln-1 with allyl-*α*-KO bound. Residues involved in calcium ion coordination and ligand binding are noted. Dashed lines show heptavalent coordination of the calcium ion. (c) Rotation of the binding pocket shows a hydrogen bond between KO and W288, depicted by a dashed line ($r_{NH\cdots O}$ = 2.9 Å).

for Apo-hItln-1 (PDB entry 4wmq) and allyl-*β*-D-Gal*f*-bound hItln-1 (PDB entry 4wmy), the asymmetric unit of the allyl-*α*-KO-bound hItln-1 structure contains two monomers.[25] We did not observe sufficient density to model the N-terminal residues and the interchain disulfide bridge between residues Cys31 and Cys48; however, the crystal packing of the monomers is consistent with two unique trimers arranged by a crystallographic three-fold axis. The binding pocket of the monomer in chain A is solvent exposed, whereas that of the monomer in chain B is oriented such that the bound KO contacts surface residues of the chain A monomer. Although the ligands are bound in nearly identical conformations (0.28 Å RMSD over

https://dx.doi.org/10.1021/jacs.9b11699
J. Am. Chem. Soc. 2020, 142, 2386−2395

19 atoms), we focused on chain A for analysis of the bound ligand. HItln-1 binds allyl-α-KO via recognition of its exocyclic vicinal diol, with the O7 and O8 hydroxyl groups of allyl-α-KO coordinating to the calcium ion present in the hItln-1 binding site (Figure 3b). In comparison to β-Gal*f*, allyl-α-KO engages in an additional hydrogen bond between the KO C1 carboxylate group and the indole nitrogen of the hItln-1 Trp288 residue (Figure 3b), which could contribute to the higher affinity observed for KO over Gal*f*. From the IC_{50} values, the free energy of binding for KO relative to Gal*f* was estimated as $\Delta\Delta G = -0.6$ kcal/mol, which is on the scale of stabilization gained by a typical hydrogen bond.

The observed ligand density of allyl-α-KO allowed unambiguous assignment of the bound ligand conformation (Figure S5). The pyranose ring puckering of KO can be described by the Cremer−Pople parameters θ, ϕ, and Q.[34] In chain A of hItln-1, KO has θ, ϕ, and Q values of 9.5°, 264.6°, and 0.58 Å respectively, indicating a near ideal $^5C_2$ ($^4C_1$) chair conformation. The calcium-coordinating exocyclic vicinal diol is in the gauche conformation, with a dihedral angle of 51°. The torsion angle around the C6−C7 bond is trans−gauche (*tg*), and that around the C7−C8 bond is gauche−trans (*gt*). The observed conformation of the diol side chain allows the pyranose ring of KO to fit in the hItln-1 binding pocket and engage nearby polar and aromatic side chains through hydrogen bonding and CH−π interactions.

Bioinformatic Analysis of Glycan Conformation. As stated earlier, glycans generally adopt their low-energy conformation when they bind to lectins. We therefore analyzed the Protein Data Bank (PDB) to assess the bound conformations of glycans containing exocyclic vicinal diols. We performed a structure-based chemical component search of the PDB for structures with a resolution of ≤2.0 Å containing pyranose or furanose ligands with an exocyclic vicinal diol side chain at C5 or C4, respectively. We eliminated sialic acids from our search, as we previously found that hItln-1 does not bind *N*-acetyl neuraminic acid due to steric clash between the carboxyl group of the ligand the hItln-1 E274 side chain.[25] Our initial search yielded 121 hits. However, because crystallographic data on carbohydrates is notoriously prone to errors,[17] we manually assessed the electron density of each glycan. We eliminated 24 structures due to incomplete electron density for the exocyclic vicinal diol or participation in a covalent linkage. The remaining 97 structures included nine unique pyranoses and two furanoses (Table S2A).

We next determined the dihedral angles of the exocyclic diol side chain in glycans with either an axial (KO-like) or equatorial (heptose-like) hydroxyl at the C4 position (Figure 4). Calcium coordination by a saccharide demands that the two side chain hydroxyl groups are gauche; therefore, we focused on the relative orientation of the first hydroxyl group of the side chain (i.e., the C6−C7 rotamer in KDO and KO or the C5−C6 rotamer in the heptoses) to the ring. We assigned the rotamer using the convention employed for hexoses in the pyranose form, in which the orientation (gauche (*g*) or trans (*t*)) of the proximal side chain hydroxyl group is listed first relative to the ring C−O bond (g or t) and then the ring C−C bond (i.e., *tg*, *gg*, or *gt*; Figure 4a). For example, the structure of KO bound to hItln-1 reported herein was resolved in the *tg* conformation as the C7 hydroxyl group is trans to the ring C−O bond but gauche to the C5−C6 bond. We also documented interactions between the exocyclic vicinal diol and protein side chains, ligands, or metal ions to account for potential intermolecular conformational influences.

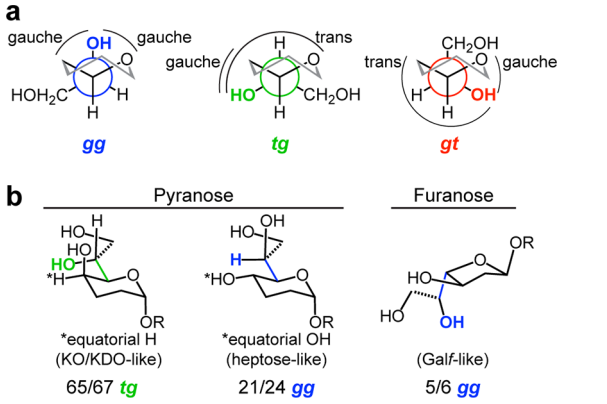

Figure 4. Bioinformatic analysis of exocyclic vicinal diol-containing glycans in the PDB. (a) Newman projections showing the *gg*, *tg*, and *gt* conformations of the proximal hydroxyl of the exocyclic vicinal diol (highlighted in blue, green, or red) with respect to the C5−O bond first, and the C5−C4 bond second (cf. C4−O and C4−C3 for furanoses). (b) The most prevalent proximal hydroxyl conformation of the three classes of carbohydrate in our analysis are shown. For pyranoses with an equatorial hydrogen, 65/67 structures are *tg*; pyranoses with an equatorial hydroxyl, 21/24 structures are *gg*; and furanoses with an equatorial hydroxyl, 5/6 structures are *gg*.

We identified distinct differences in the favored conformations of the heptoses versus those of KDO and KO. Analysis of structures with KO or KDO indicate these saccharides share a strong conformational preference. Of 67 structures, 65 had the proximal hydroxyl group of the side chain in the *tg* conformation (Figure 4, Table S2B). The aberrant structures were in the *gg* conformation—a preference driven by the simultaneous coordination of KDO carboxylate and the axial hydroxyl and C7 side chain hydroxyl groups to a calcium ion.[35] The predominant *tg* conformation is that observed for KO bound to hItln-1. A similar analysis of the heptose sugars revealed their conformational preferences differ from those of KDO and KO. Of the 24 heptose structures, the majority include L,D-heptose in a proximal *gg* conformation (21), while three had D,D-heptose in the *gt* conformation (Figure 4, Table S2B). These observations indicate that the configuration of the side chain hydroxyl group impacts the conformation and that the predominant conformations of heptoses and KDO/KO diverge dramatically.

We also analyzed furanose structures, though far fewer were available. The majority of proximal hydroxyl groups in these cases (five of six) occupied the *gg* conformation (Table S2B). The one exception had three hydrogen bonds involving the proximal hydroxyl group, likely influencing the conformation.[36] The preferred *gg* conformation is that present in the structure of hItln-1 bound to β-Gal*f*. The bioinformatic analysis was striking in that each saccharide residue was found to adopt a preferred conformation in which the orientation of the glycan side chain and the pyranose or furanose was defined.

Computational Analysis of Glycan Conformation and Recognition. We examined whether the preferred conformations of the heptoses would be compatible with hItln-1 binding by employing modeling and computational methods. We extracted coordinates of L,D- and D,D-heptose bound to surfactant protein D (SP-D; PDB entries 2rib and 2ria, respectively),[37] a C-type lectin. The heptose-bound con-

https://dx.doi.org/10.1021/jacs.9b11699
J. Am. Chem. Soc. 2020, 142, 2386−2395

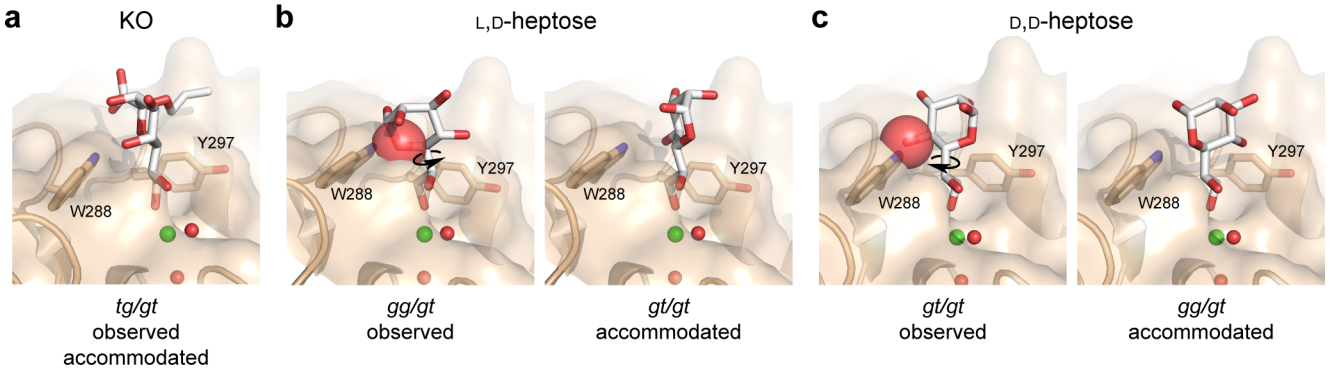

Figure 5. Observed and accommodated ligand conformations in hItln-1 binding site. (a) KO can bind to hItln-1 in the *tg*/*tg* conformation without steric interactions, as observed in the structure of the complex (Figure 3). Alignment of the exocyclic vicinal diol of L,D-heptose (b) or D,D-heptose (c) affords steric interaction between each ligand and W288, depicted by red spheres. Rotation about the proximal bond of the exocyclic vicinal diol side chain gives rise to ligand conformations accommodated by the hItln-1 binding site without steric interaction. Ligands are shown in white sticks, and red spheres represent the van der Waals radii of atoms with significant interactions. Observed conformations of L,D-heptose and D,D-heptose were extracted from PDB entries 2rib and 2ria, respectively.

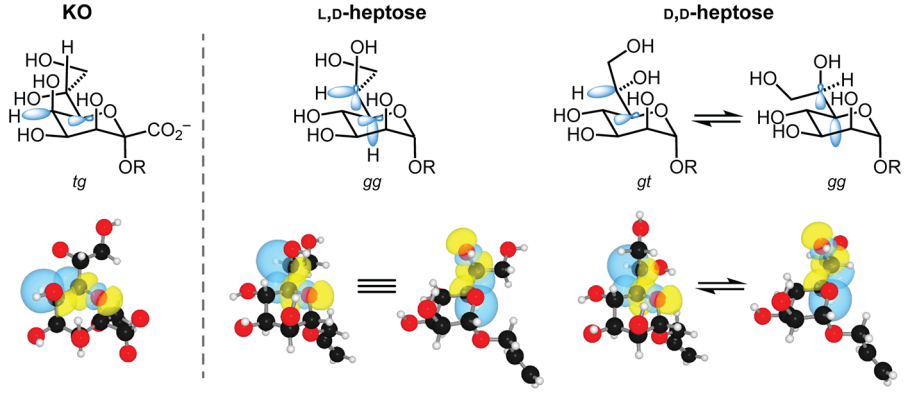

Figure 6. Stabilizing stereoelectronic effects of preferred rotamers of the proximal side chain C−C bond of KO, L,D-heptose, and D,D-heptose. Preferred rotamers are based on predominant conformations in published PDB structures. Relevant orbitals involved in stabilizing these conformations are represented in blue (top). NBO renderings of significant $\sigma_{C-H} \rightarrow \sigma^*_{C-O}$ interactions are depicted with blue and yellow orbitals (bottom). Rotamers shown were atom-optimized at the M06-2X/6-311+G(d,p) level of theory employing the IEFPCM solvation model. For clarity, two separate renderings are shown for each stabilizing interaction in the preferred *gg* L,D-heptose conformer. Comparisons of these interactions aid in explaining the differences in affinity of each monosaccharide to hItln-1.

formations in these structures are representative of those that predominated in our PDB analysis. We aligned the exocyclic vicinal diol with that of KO bound to hItln-1 by rigid-body superimposition. The preferred conformers of each heptose would experience significant steric repulsion from the protein surface, precluding binding to hItln-1 (Figure 5). By rotating around the C5−C6 exocyclic bond, we identified single conformations of each that are permissive for binding (Figure 5). The *gt* conformer of L,D-heptose is the sole rotamer that fits in the binding pocket without steric clashes. For D,D-heptose, the *gg* conformer is the only one accommodated. The heptose conformations were not those that dominated in our bioinformatic analysis (i.e., *gt* for D,D-heptose, and *gg* for L,D-heptose). Thus, our analysis predicts the affinities observed for hItln-1 binding.

The observed differences in side chain conformation between KO/KDO and the heptoses suggested that substituents on the saccharide ring are influential. KDO and KO have an axial hydroxyl group at the 5-position, while the corresponding C4 hydroxyl group in the heptoses is equatorial. We postulated that this position would impart sterics and stereoelectronic effects. To this end, we performed all-atom optimizations of the observed conformation of the heptose structures as well as the conformers accommodated by the hItln-1 binding site using density functional theory (DFT). We reasoned that the preferred conformers would be stabilized by hyperconjugation, so we employed natural bonding orbital (NBO) analysis to assess the energies of the various rotamers. We examined whether altered donation to the ring σ^*_{C-O} antibonding orbitals might influence side chain orientation. For the heptoses, we summed the interaction energies for donation to the ring oxygen (C5−O) and the proximal exocyclic hydroxyl group (C6−O) σ^*_{C-O} orbitals for the observed and hItln-1-accommodated structures (Figure 6, Table S4). We also added the interaction energies with the exchanged donors and alternative acceptors (Table S4). In this way, we estimate that the *gt* conformer (the major rotamer observed in the PDB) and *gg* (hItln-1 accommodating) are similar in energy (0.2 kcal/mol) for D,D-heptose but L,D-heptose prefers the *gg* (by 3.3 kcal/mol). The computationally derived values in Table S4 are on par with previously published values.[38] The low energy L,D-heptose conformation is incompatible with hItln-1 complexation. This analysis is consistent with the binding data indicating D,D-heptose is a better hItln-1 ligand. We also performed all-atom optimizations with DFT and NBO analysis of the hItln-1 ligand, KO

https://dx.doi.org/10.1021/jacs.9b11699
J. Am. Chem. Soc. 2020, 142, 2386−2395

(Figure 6, Table S3). KO benefits from a fixed equatorial C−H bond at C5, which can donate into the ring σ^*_{C-O} orbital. The side chain therefore adopts a conformation that minimizes steric interactions and is aligned for hItln-1 binding. These calculations predict the low-energy conformation found in the PDB and the hItln-1 structure.

DISCUSSION

Lectin−glycan interactions are critical in innate immunity. We are intrigued by the possibility that host lectins detect and control microbial populations. To understand and predict protein−carbohydrate recognition, we analyzed hItln-1−glycan interactions to elucidate features of sugars that influence lectin affinity. HItln-1 recognizes multiple glycans that possess glyceryl side chains. As a consequence, studying hItln-1 provides an opportunity to examine the interplay of saccharide steric and stereoelectronic effects that influence lectin binding. We determined that heptoses bind more weakly than KO, KDO, or β-Gal*f*. That heptoses and *N*-acetylneuraminic acid are poor hItln-1 ligands underscores that a terminal 1,2-diol is not sufficient. HItln-1 can distinguish between saccharides that possess the critical glyceryl group. Among carbohydrates exclusively utilized by microbes, L,D-heptose is the most commonly observed monosaccharide building block.[31] Indeed, this saccharide is widely distributed throughout Gram negative bacteria and is a critical component of many lipopolysaccharides. The ability of hItln-1 to discriminate against L,D-heptose could augment the lectin's selectivity for distinct microbial species.

A molecular understanding of X-type lectin binding emerged with the determination of the structures of hItln-1 bound to allyl-β-D-Gal*f*[25] and the frog lectin XEEL complexed with glycerol-1-phosphate.[26] In each of these structures, the terminal 1,2-diol of the ligand coordinates to the protein-bound calcium ion. The structure of hItln-1 bound to KO reinforces the importance of exocyclic diol coordination. This structure alone, however, does not explain why L,D-heptose binds so weakly. The molecular basis for the disparity in affinity between L,D- and D,D-heptose epimers was not apparent. Because saccharides that are pre-organized for lectin binding (i.e., can interact via their low-energy conformation) should be the most effective ligands, we hypothesized that the low-energy conformations of KO and KDO would enable binding but that of L,D-heptose would be incompatible.

To test this hypothesis, we employed a meta-analysis of high-resolution structures in the PDB. We examined the structures of candidate glycans that possess the terminal 1,2-diol, including KO, KDO, and the heptoses. Although the monosaccharide units were crystallized in a variety of different chemical environments, distinct conformations predominated. The ulosonic acids KO and KDO (and related sugars) are almost always (97%) in the conformation observed in the hItln-1·KO complex. In contrast, the prevalent heptose conformations are not those that are poised for hItln-1 binding.

Glucose and galactose, which are epimeric at the C4 position, have been observed to populate different ω angles driven by sterics, solvent interactions, and stereoelectronic effects.[14,39] The data presented herein suggest that in monosaccharides with higher substitution at the C6-equivalent position, the conformation of the proximal side chain hydroxyl group depends on the configuration of the adjacent ring hydroxyl group (C4 in heptoses; C5 in KO/KDO) and the stereochemistry of the exocyclic hydroxyl group itself. The preferences observed are reinforced not only by sterics but also by stereoelectronic effects. In carbohydrates, the ring C−O bond is most electron deficient due to the anomeric $n_O \rightarrow \sigma^*_{C-O}$ interaction and the inductive effect. The system is stabilized by donation into the ring σ^*_{C-O} orbital, which can come from an electron-rich σ_{C-H} orbital. In KO/KDO, the equatorial C5−H is aligned for hyperconjugation. The proximal side chain bond then adopts the sterically preferred *tg* conformation. Here, the alignment of the smallest group (H) with the axial hydroxyl group is preferable to a 1,3-diaxial interaction of hydroxyl groups. Thus, stereoelectronic and steric effects stabilize the hItln-1-bound conformation, and this conformation is present in 65 of 67 PDB structures.

In contrast to KDO and KO, L,D- and D,D-heptose have an equatorial hydroxyl group at C4. Accordingly, the conformation that provides hyperconjugative stabilization is one in which the C−H bond of the side chain is aligned to donate electron density into the ring σ^*_{C-O} orbital. Our analysis of PDB structures and the NBO calculations indicate that the *gg* rotamer is the preferred and prevalent conformation of L,D-heptose. The L,D-heptose *gg* conformation is stabilized further by a second orbital overlap of the C5 σ_{C-H} orbital of the ring to the C6 side chain hydroxyl σ^*_{C-O} orbital. This rotamer also avoids unfavorable syn pentane interactions that would occur in other conformations. Superposition-based docking of the preferred conformation of L,D-heptose ligand into the binding site indicates a steric clash with Trp288 and a poor fit. Our *in silico* conformational analysis predicts that the heptose conformer that could accommodate hItln-1 binding is energetically disfavored.

For D,D-heptose, no single rotamer both avoids unfavorable steric interactions and capitalizes on stabilizing stereoelectronic interactions. Indeed, the *gt* and *gg* conformations are roughly equal in calculated energy. The NBO analysis accounts for the electronic contribution, however, the *gg* conformation of D,D-heptose would experience a steric effect similar to a 1,3-diaxial interaction and has a C−C rather than C−H bond donating into the σ^*_{C-O} orbital. Of the two D,D-heptose rotamers favored by stereoelectronics, binding of the *gt* rotamer is precluded by a steric clash with Trp288, whereas the *gg* rotamer could be docked in the hItln-1 binding site. These analyses would predict that D,D-heptose is a better hItln-1 ligand than is L,D-heptose, a prediction consistent with the binding data. Still, D,D-heptose lacks the benefits of preorganization intrinsic to KO and KDO. The difference in rotamer preference observed for each of the bacterial glycans studied herein is consistent with previous observations that side chain conformation influences glycosylation reactions.[15]

The difference in affinity for monomeric D,D-heptose versus Gal*f* binding appears small, yet we see no binding to immobilized D,D-heptose in an ELISA (Figure 2). The discrimination between D,D-heptose and β-Gal*f* arises from multivalent interactions, whereby small differences in binding are amplified.[30] Thus, through stereoelectronic effects and multivalent binding hItln-1 binds selectively to surfaces displaying KDO/KO, 1-phospho-glycerol, and β-Gal*f*.

We find that hItln-1 binding to microbial sugars is determined by the recognition of an exocyclic diol, but our results indicate that the diol conformation and its relationship relative to the saccharide ring are major determinants of selectivity. The differential recognition of monosaccharides we observe could not have been predicted from the glycan array results alone. Many other lectins have known monosaccharide

https://dx.doi.org/10.1021/jacs.9b11699
J. Am. Chem. Soc. 2020, 142, 2386−2395

ligands or binding epitopes but a detailed analysis of the structural and conformational constraints that determine affinity and selectivity is lacking. For example, L-ficolin is proposed to bind glycans with a simple acetyl group motif, but this lectin displays a range of affinities across monosaccharides containing this epitope.[40,41] Our molecular analysis afforded a more complete ligand binding profile of hItln-1, which can guide future investigations into the function of this lectin and provide a basis for understanding the specificity of lectin−glycan interactions.

CONCLUSION

Our studies illuminate how saccharide conformation influences lectin specificity. Whereas carbohydrates are often viewed as conformationally flexible molecules, stereoelectronic effects, such as the gauche effect, are critical determinants of conformational preferences. Because lectins typically bind the low-energy conformations of glycans, we used X-ray crystallography and bioinformatic analysis to assess the favored rotamers of the ulosonic acids KO and KDO, β-Gal*f*, and the heptoses. Though the differences in binding affinity were subtle on the monosaccharide level, these preferences were amplified upon the binding of the trimeric hItln-1 to a surface displaying a target ligand. In such a multivalent assay, hItln-1 bound to Gal*f*, KDO, and KO but not to either L-D-heptose or D-D-heptose. We anticipate that this specificity is critical for the physiological function of hItln-1 and will aid in the prediction, analysis, and generation of synthetic lectin ligands. These advances in our understanding of lectin−glycan interactions should also facilitate the generation of effective lectin inhibitors.

MATERIALS AND METHODS

Recombinant Protein Expression. Recombinant hItln-1 with an N-terminal *Strep*-tag II (IBA Lifesciences) was expressed via transient transfection of suspension adapted HEK293 cells as previously described.[25] Purification was performed as described using *Strep*-Tactin Superflow high capacity resin (IBA Lifesciences, cat. no. 2-1208-002). The concentration of *Strep*-hItln-1 was determined by absorbance at 280 nm, with a calculated ε = 239 775 M^{-1} cm^{-1} and a molecular mass of 102 024 Da for the disulfide-linked trimer.

Protein for X-ray Crystallography. *Strep*-hItln-1 was expressed and purified as previously described with minor modifications.[25] Conditioned expression medium was harvested by centrifugation and sterile filtration. The culture medium was then adjusted to pH 6.7 by slow addition of 0.1 M sodium hydroxide, avidin was added per the IBA protocol, calcium chloride was added to 10 mM, and the solution was cleared by centrifugation. Protein purification was performed by capture onto *Strep*-Tactin Superflow high-capacity resin, washed with 20 mM bis-Tris, pH 6.7, 150 mM sodium chloride, and 1 mM EDTA; eluted with 5 mM *d*-desthiobiotin (Sigma) in 20 mM bis-Tris, pH 6.7, 150 mM sodium chloride, and 1 mM EDTA and concentrated with a 30,000-MWCO Amicon Ultra centrifugal filter.

Chemical Synthesis of Glycans. Detailed information on synthesis and characterization can be found in the Supporting Information.

Biolayer Interferometry (BLItz). IC_{50} values for monosaccharides with hItln-1 were determined using a BLItz instrument (ForteBio). Biotin-Gal*f* was loaded (300 s) onto streptavidin biosensors as a 5 μM solution in phosphate-buffered saline (PBS). The sensor was washed in HEPES-T + BSA buffer for 60 s (20 mM HEPES, pH 7.4, 150 mM sodium chloride, 10 mM calcium chloride, 0.1% Tween-20, 0.1% BSA). hItln-1 was then associated (15 μg/mL in association buffer) for 300 s in the presence of various concentrations of competitor monosaccharide (0 to 100 mM), followed by dissociation in HEPES-T + bovine serum albumin (BSA) buffer for 90 s. The shake rate was set to 1000 rpm throughout the experiment and all reagents were used at room temperature. Data was adjusted based on a reference curve (no hItln-1 in association step). The last 10 s of association (710−720 s) were averaged together, normalized, and plotted as a curve of % binding of hItln-1 to Gal*f* vs log [competitor] (mM). Data were analyzed in Prism8 (GraphPad) and fitted to a one-site log IC_{50} equation.

ELISA. Monosaccharides conjugated to BSA were adsorbed onto a Maxisorp (Nunc) flat-bottomed 96-well plate in phosphate buffered saline (PBS) (1.5 μM by sugar concentration present) and incubated at room temperature for 1 h. After washing with PBS (3 × 5 min), wells were then blocked with 5% w/v BSA in HEPES-T buffer for 2 h. The plate was washed with HEPES-T buffer (3 × 5 min) and then *Strep*-hItln-1 solutions prepared by serial dilution into HEPES-T + BSA buffer were added to wells for 2 h at room temperature. Wells were washed 4 times with HEPES-T buffer and then incubated with *Strep*MAB-Classic HRP conjugate (IBA, cat. no. 2-1509-001; 1:10 000 dilution in HEPES-T + BSA) for 2 h at room temperature for detection of the *Strep*-tag II of bound hItln-1. Wells were washed with HEPES-T (3 × 5 min) and hItln-1 was detected colorimetrically by addition of 1-Step Ultra TMB-ELISA and quenching with an equal volume of 2 M sulfuric acid. Plates were read at 450 nm on an ELx800 plate reader (Bio-Tek). Data were analyzed in Prism8 (GraphPad) and fitted to a one-site binding equation.

Protein X-ray Crystallography. *Protein Crystallization.* The *Strep*-hItln-1 protein that was purified with 20 mM bis-Tris, pH 6.7, was concentrated to 1.5 mg/mL, 1 M $CaCl_2$ was added to 10 mM. Crystallization was performed in 100 mM bis-Tris, pH 6.0, and 25% PEG 3350 (hanging drop) as previously described.[25] Crystals grew to full size in 5 weeks, and additional crystals continued to appear over the next 2 months. The allyl-α-KO complex was formed by soaking of apo-hItln-1 crystals in cryoprotection solution (100 mM bis-Tris, pH 6.0, 35% PEG 3350) supplemented with 50 mM allyl-α-KO for 7 days prior to cryopreservation.

X-ray Diffraction. Single crystal diffraction experiments were performed at beamline 23-ID-B equipped with Dectris Eiger-16m detector (GM/CA, Advanced Photon Source, Argonne National Laboratory). Data were indexed and integrated with DIALS and scaled with Aimless.[42] Details of X-ray diffraction experiments and ensuing data are found in Table S1.

Structure Solution and Refinement. The monomer from chain A of the hItln-1 apo structure (PDB 4wmq) with alternative conformations removed was used as an input for molecular replacement. Molecular replacement was conducted using Phaser implemented in PHENIX.[43] Model building including the fitting of protein, solvent, and ligands was conducted with COOT.[44] Refinement was conducted with phenix.refine using PHENIX. The initial model of the ligand, prop-2-en-1-yl D-*glycero*-α-D-*talo*-oct-2-ulopyranosidonic acid (KO), was obtained from the PDB (ligand code: ko2). Restraints were prepared with eLBOW as implemented in PHENIX. The Protein Data Bank accession code for the deposited coordinates and structure factors of hItln-1 bound to allyl-KO is 6USC.

Bioinformatics. The PDB was queried for pyranoses and furanoses containing an exocyclic diol at the C5 or C4 position, respectively, using the structure-based chemical component search tool. Resulting structures resolved at ≤2.0 Å were analyzed manually to determine completeness of ligand density and assignment of the exocyclic diol conformation. First, the $2F_o - F_c$ map contoured at 1.5σ was examined for each individual carbohydrate ligand using the Electron Density Map feature of the 3D View tool found on the PDB Web site to ensure electron density was present for the side chain and that the ligand was accurately fitted to the density. If the electron density was absent for part of the molecule, the structure was omitted from our analysis. Additionally, any ligands where either hydroxyl of the exocyclic diol was participating in a covalent linkage were omitted. Next, the conformation of the exocyclic diol was recorded (Table S2A) for the proximal hydroxyl group (i.e., the one most proximal to the ring) and the distal hydroxyl group (i.e., the terminal one). Each rotamer is assigned by the gauche or trans orientation of the O−C−

https://dx.doi.org/10.1021/jacs.9b11699
J. Am. Chem. Soc. 2020, 142, 2386−2395

C−O and O−C−C−C dihedral angels using the gauche−trans (*gt*), gauche−gauche (*gg*), trans−gauche (*tg*) annotation. Finally, interactions autonomously identified using the Ligand View feature of the 3D View tool were recorded to account for potential influences on conformation (Table S2A).[45]

Computational Analysis. *DFT Optimization with Gaussian.* Full structure optimizations were conducted with Gaussian 16, Revision A.03 software from Gaussian (Wallingford, CT).[46] Initial structures were prepared with GaussView 6.0 (Gaussian). Optimizations were conducted at the M06-2X/6-311+G(d,p) level of theory employing the IEFPCM solvation model. Structures with several intramolecular hydrogen bonding patterns were optimized for the sugar in the conformation found in co-crystal structures with lectins to identify the lowest energy hydrogen atom conformation. Additional models were prepared to access the consequences of changing the conformation of non-hydrogen atoms. Again, several conformations were sampled for the hydrogens on mobile atoms to identify the minimum energy conformer. Minimized structures were confirmed to lack imaginary frequencies.

Natural Bonding Orbital Analysis. NBO analysis was conducted using NBO 6.0 software.[47] Reported energies for donor−acceptor interactions were calculated by second-order perturbation analysis. Changes in energy for bond rotation (ΔE_{NBO}) were calculated by summing the energies of donor−acceptor interactions between NBOs associated with atoms of the rotated bonds that have altered interactions during the rotation and finding the difference in unique stabilizing energy between the two rotamers (Table S4). 3D images of orbital overlaps were rendered using NBOView 1.1 software.

■ ASSOCIATED CONTENT

Supporting Information

The Supporting Information is available free of charge at https://pubs.acs.org/doi/10.1021/jacs.9b11699.

Supporting Figures S1−S5 and Tables S1−S4, synthetic procedures, ^{1}H and ^{13}C NMR spectra, and MALDI spectra of BSA conjugates (PDF)

■ AUTHOR INFORMATION

Corresponding Author

Laura L. Kiessling − *Department of Chemistry, Massachusetts Institute of Technology, Cambridge, Massachusetts 02139, United States;* orcid.org/0000-0001-6829-1500; Email: kiesslin@mit.edu

Authors

Caitlin M. McMahon − *Department of Chemistry, Massachusetts Institute of Technology, Cambridge, Massachusetts 02139, United States*

Christine R. Isabella − *Department of Chemistry, Massachusetts Institute of Technology, Cambridge, Massachusetts 02139, United States;* orcid.org/0000-0003-0786-7240

Ian W. Windsor − *Department of Chemistry, Massachusetts Institute of Technology, Cambridge, Massachusetts 02139, United States;* orcid.org/0000-0002-6289-6928

Paul Kosma − *Department of Chemistry, University of Natural Resources and Life Sciences, A-1190 Vienna, Austria;* orcid.org/0000-0001-5342-7161

Ronald T. Raines − *Department of Chemistry, Massachusetts Institute of Technology, Cambridge, Massachusetts 02139, United States;* orcid.org/0000-0001-7164-1719

Complete contact information is available at: https://pubs.acs.org/10.1021/jacs.9b11699

Author Contributions

§C.M.M. and C.R.I. contributed equally.

Notes

The authors declare no competing financial interest.

■ ACKNOWLEDGMENTS

Research reported in this publication was supported by the National Institute of Allergy and Infectious Diseases under grant number R01 AI055258 (L.L.K.), the National Cancer Institute under grant number U01 CA2310789 (L.L.K.), the National Institute of General Medical Sciences R01 GM044783 (R.T.R.), and the Austrian Science Fund FWF (P 28826-N28, P.K.). We acknowledge NIGMS F32 GM125165 (C.M.M.) and National Science Foundation Graduate Research Fellowship Program 1122374 (C.R.I.) for fellowships. We thank Craig Bingman (Collaborative Crystallography Core in the Department of Biochemistry, University of Wisconsin−Madison) for data collection and Craig Ogata (GM/CA@APS) for beamline support. This research has made use of GM/CA@APS, which has been funded by National Cancer Institute (ACB-12002) and the NIGMS (AGM-12006). This research used resources of the Advanced Photon Source, a U.S. Department of Energy (DOE) Office of Science User Facility operated for the DOE Office of Science by Argonne National Laboratory under Contract No. DE-AC02-06CH11357. The Eiger 16M detector was funded by an NIH−Office of Research Infrastructure Programs, High-End Instrumentation Grant (1S10OD012289-01A1). This work utilized the Molecular Graphics and Computation Facility at the University of California−Berkeley, which is funded by Grant NIH S10OD023532. We also thank Prof. Barbara Imperiali (Massachusetts Institute of Technology) for providing generous access to equipment and Bob Dass (Pall) for advice and assistance with instrumentation.

■ REFERENCES

(1) Lee, Y. C.; Lee, R. T. Carbohydrate-Protein Interactions: Basis of Glycobiology. *Acc. Chem. Res.* **1995**, *28* (8), 321−327.

(2) Bewley, C. A. *Protein−Carbohydrate Interactions in Infectious Diseases*; RSC Publishing: Cambridge, UK, 2006.

(3) Lis, H.; Sharon, N. Lectins: Carbohydrate-Specific Proteins That Mediate Cellular Recognition. *Chem. Rev.* **1998**, *98* (2), 637−674.

(4) Varki, A. Biological roles of glycans. *Glycobiology* **2017**, *27* (1), 3−49.

(5) Weis, W. I.; Drickamer, K. Structural basis of lectin-carbohydrate recognition. *Annu. Rev. Biochem.* **1996**, *65*, 441−473.

(6) Elgavish, S.; Shaanan, B. Lectin-carbohydrate interactions: different folds, common recognition principles. *Trends Biochem. Sci.* **1997**, *22* (12), 462−467.

(7) Gabius, H.-J.; André, S.; Jiménez-Barbero, J.; Romero, A.; Solís, D. From lectin structure to functional glycomics: principles of the sugar code. *Trends Biochem. Sci.* **2011**, *36* (6), 298−313.

(8) Park, S.; Gildersleeve, J. C.; Blixt, O.; Shin, I. Carbohydrate microarrays. *Chem. Soc. Rev.* **2013**, *42* (10), 4310−4326.

(9) Wesener, D. A.; Dugan, A.; Kiessling, L. L. Recognition of microbial glycans by soluble human lectins. *Curr. Opin. Struct. Biol.* **2017**, *44*, 168−178.

(10) Imberty, A.; Pérez, S. Structure, Conformation, and Dynamics of Bioactive Oligosaccharides: Theoretical Approaches and Experimental Validations. *Chem. Rev.* **2000**, *100* (12), 4567−4588.

(11) Asensio, J. L.; Ardá, A.; Cañada, F. J.; Jiménez-Barbero, J. Carbohydrate-Aromatic Interactions. *Acc. Chem. Res.* **2013**, *46* (4), 946−954.

(12) Hudson, K. L.; Bartlett, G. J.; Diehl, R. C.; Agirre, J.; Gallagher, T.; Kiessling, L. L.; Woolfson, D. N. Carbohydrate-Aromatic

Interactions in Proteins. *J. Am. Chem. Soc.* **2015**, *137* (48), 15152−15160.
(13) Kiessling, L. L. Chemistry-driven glycoscience. *Bioorg. Med. Chem.* **2018**, *26* (19), 5229−5238.
(14) Woods, R. J. Predicting the Structures of Glycans, Glycoproteins, and Their Complexes. *Chem. Rev.* **2018**, *118* (17), 8005−8024.
(15) Moumé-Pymbock, M.; Furukawa, T.; Mondal, S.; Crich, D. Probing the Influence of a 4,6-*O*-Acetal on the Reactivity of Galactopyranosyl Donors: Verification of the Disarming Influence of the trans−gauche Conformation of C5−C6 Bonds. *J. Am. Chem. Soc.* **2013**, *135* (38), 14249−14255.
(16) Wormald, M. R.; Petrescu, A. J.; Pao, Y.-L.; Glithero, A.; Elliott, T.; Dwek, R. A. Conformational Studies of Oligosaccharides and Glycopeptides: Complementarity of NMR, X-ray Crystallography, and Molecular Modelling. *Chem. Rev.* **2002**, *102* (2), 371−386.
(17) Agirre, J.; Davies, G.; Wilson, K.; Cowtan, K. Carbohydrate anomalies in the PDB. *Nat. Chem. Biol.* **2015**, *11*, 303.
(18) Nivedha, A. K.; Makeneni, S.; Foley, B. L.; Tessier, M. B.; Woods, R. J. Importance of ligand conformational energies in carbohydrate docking: Sorting the wheat from the chaff. *J. Comput. Chem.* **2014**, *35* (7), 526−539.
(19) Suzuki, Y. A.; Shin, K.; Lönnerdal, B. Molecular Cloning and Functional Expression of a Human Intestinal Lactoferrin Receptor. *Biochemistry* **2001**, *40* (51), 15771−15779.
(20) Tsuji, S.; Uehori, J.; Matsumoto, M.; Suzuki, Y.; Matsuhisa, A.; Toyoshima, K.; Seya, T. Human Intelectin Is a Novel Soluble Lectin That Recognizes Galactofuranose in Carbohydrate Chains of Bacterial Cell Wall. *J. Biol. Chem.* **2001**, *276* (26), 23456−23463.
(21) Voehringer, D.; Stanley, S. A.; Cox, J. S.; Completo, G. C.; Lowary, T. L.; Locksley, R. M. *Nippostrongylus brasiliensis*: Identification of intelectin-1 and −2 as Stat6-dependent genes expressed in lung and intestine during infection. *Exp. Parasitol.* **2007**, *116* (4), 458−466.
(22) Barrett, J. C; Hansoul, S.; Nicolae, D. L; Cho, J. H; Duerr, R. H; Rioux, J. D; Brant, S. R; Silverberg, M. S; Taylor, K. D; Barmada, M M.; Bitton, A.; Dassopoulos, T.; Datta, L. W.; Green, T.; Griffiths, A. M; Kistner, E. O; Murtha, M. T; Regueiro, M. D; Rotter, J. I; Schumm, L P.; Steinhart, A H.; Targan, S. R; Xavier, R. J; Libioulle, C.; Sandor, C.; Lathrop, M.; Belaiche, J.; Dewit, O.; Gut, I.; Heath, S.; Laukens, D.; Mni, M.; Rutgeerts, P.; Van Gossum, A.; Zelenika, D.; Franchimont, D.; Hugot, J.-P.; de Vos, M.; Vermeire, S.; Louis, E.; Cardon, L. R; Anderson, C. A; Drummond, H.; Nimmo, E.; Ahmad, T.; Prescott, N. J.; Onnie, C. M; Fisher, S. A; Marchini, J.; Ghori, J.; Bumpstead, S.; Gwilliam, R.; Tremelling, M.; Deloukas, P.; Mansfield, J.; Jewell, D.; Satsangi, J.; Mathew, C. G; Parkes, M.; Georges, M.; Daly, M. J Genome-wide association defines more than 30 distinct susceptibility loci for Crohn's disease. *Nat. Genet.* **2008**, *40* (8), 955−962.
(23) de Souza Batista, C. M.; Yang, R.-Z.; Lee, M.-J.; Glynn, N. M.; Yu, D.-Z.; Pray, J.; Ndubuizu, K.; Patil, S.; Schwartz, A.; Kligman, M.; Fried, S. K.; Gong, D.-W.; Shuldiner, A. R.; Pollin, T. I.; McLenithan, J. C. Omentin Plasma Levels and Gene Expression Are Decreased in Obesity. *Diabetes* **2007**, *56* (6), 1655−1661.
(24) Kerr, S. C.; Carrington, S. D.; Oscarson, S.; Gallagher, M. E.; Solon, M.; Yuan, S.; Ahn, J. N.; Dougherty, R. H.; Finkbeiner, W. E.; Peters, M. C.; Fahy, J. V. Intelectin-1 Is a Prominent Protein Constituent of Pathologic Mucus Associated with Eosinophilic Airway Inflammation in Asthma. *Am. J. Respir. Crit. Care Med.* **2014**, *189* (8), 1005−1007.
(25) Wesener, D. A.; Wangkanont, K.; McBride, R.; Song, X.; Kraft, M. B.; Hodges, H. L.; Zarling, L. C.; Splain, R. A.; Smith, D. F.; Cummings, R. D.; Paulson, J. C.; Forest, K. T.; Kiessling, L. L. Recognition of microbial glycans by human intelectin-1. *Nat. Struct. Mol. Biol.* **2015**, *22* (8), 603−610.
(26) Wangkanont, K.; Wesener, D. A.; Vidani, J. A.; Kiessling, L. L.; Forest, K. T. Structures of Xenopus Embryonic Epidermal Lectin Reveal a Conserved Mechanism of Microbial Glycan Recognition. *J. Biol. Chem.* **2016**, *291* (11), 5596−5610.
(27) Alexander, C.; Rietschel, E. T. Invited review: Bacterial lipopolysaccharides and innate immunity. *J. Endotoxin Res.* **2001**, *7* (3), 167−202.
(28) Kirschner, K. N.; Woods, R. J. Solvent interactions determine carbohydrate conformation. *Proc. Natl. Acad. Sci. U. S. A.* **2001**, *98* (19), 10541−10545.
(29) Kiessling, L. L.; Grim, J. C. Glycopolymer probes of signal transduction. *Chem. Soc. Rev.* **2013**, *42* (10), 4476−4491.
(30) Mortell, K. H.; Weatherman, R. V.; Kiessling, L. L. Recognition Specificity of Neoglycopolymers Prepared by Ring-Opening Metathesis Polymerization. *J. Am. Chem. Soc.* **1996**, *118* (9), 2297−2298.
(31) Herget, S.; Toukach, P. V.; Ranzinger, R.; Hull, W. E.; Knirel, Y. A.; von der Lieth, C.-W. Statistical analysis of the Bacterial Carbohydrate Structure Data Base (BCSDB): Characteristics and diversity of bacterial carbohydrates in comparison with mammalian glycans. *BMC Struct. Biol.* **2008**, *8*, 35.
(32) Mann, D. A.; Kanai, M.; Maly, D. J.; Kiessling, L. L. Probing Low Affinity and Multivalent Interactions with Surface Plasmon Resonance: Ligands for Concanavalin A. *J. Am. Chem. Soc.* **1998**, *120* (41), 10575−10582.
(33) Fu, Y.; Baumann, M.; Kosma, P.; Brade, L.; Brade, H. A synthetic glycoconjugate representing the genus-specific epitope of chlamydial lipopolysaccharide exhibits the same specificity as its natural counterpart. *Infect. Immun.* **1992**, *60* (4), 1314−1321.
(34) Cremer, D.; Pople, J. A. A General Definition of Ring Puckering Coordinates. *J. Am. Chem. Soc.* **1975**, *97* (6), 1354−1358.
(35) Arunmanee, W.; Pathania, M.; Solovyova, A. S.; Le Brun, A. P.; Ridley, H.; Baslé, A.; van den Berg, B.; Lakey, J. H. Gram-negative trimeric porins have specific LPS binding sites that are essential for porin biogenesis. *Proc. Natl. Acad. Sci. U. S. A.* **2016**, *113* (34), E5034−E5043.
(36) Horler, R. S. P.; Müller, A.; Williamson, D. C.; Potts, J. R.; Wilson, K. S.; Thomas, G. H. Furanose-specific Sugar Transport: Characterization of a bacterial galactofuranose binding protein. *J. Biol. Chem.* **2009**, *284* (45), 31156−31163.
(37) Wang, H.; Head, J.; Kosma, P.; Brade, H.; Müller-Loennies, S.; Sheikh, S.; McDonald, B.; Smith, K.; Cafarella, T.; Seaton, B.; Crouch, E. Recognition of Heptoses and the Inner Core of Bacterial Lipopolysaccharides by Surfactant Protein D. *Biochemistry* **2008**, *47* (2), 710−720.
(38) Martins, F. A.; Freitas, M. P. The Fluorine *gauche* Effect and a Comparison with Other Halogens in 2-Halofluoroethanes and 2-Haloethanols. *Eur. J. Org. Chem.* **2019**, *2019*, 6401−6406.
(39) Barnett, C. B.; Naidoo, K. J. Stereoelectronic and Solvation Effects Determine Hydroxymethyl Conformational Preferences in Monosaccharides. *J. Phys. Chem. B* **2008**, *112* (48), 15450−15459.
(40) Krarup, A.; Mitchell, D. A.; Sim, R. B. Recognition of acetylated oligosaccharides by human L-ficolin. *Immunol. Lett.* **2008**, *118* (2), 152−156.
(41) Krarup, A.; Thiel, S.; Hansen, A.; Fujita, T.; Jensenius, J. C. L-ficolin Is a Pattern Recognition Molecule Specific for Acetyl Groups. *J. Biol. Chem.* **2004**, *279* (46), 47513−47519.
(42) Winter, G.; Waterman, D. G.; Parkhurst, J. M.; Brewster, A. S.; Gildea, R. J.; Gerstel, M.; Fuentes-Montero, L.; Vollmar, M.; Michels-Clark, T.; Young, I. D.; Sauter, N. K.; Evans, G. DIALS: implementation and evaluation of a new integration package. *Acta Crystallogr., Sect. D: Biol. Crystallogr.* **2018**, *74* (2), 85−97.
(43) Adams, P. D.; Afonine, P. V.; Bunkóczi, G.; Chen, V. B.; Davis, I. W.; Echols, N.; Headd, J. J.; Hung, L.-W.; Kapral, G. J.; Grosse-Kunstleve, R. W.; McCoy, A. J.; Moriarty, N. W.; Oeffner, R.; Read, R. J.; Richardson, D. C.; Richardson, J. S.; Terwilliger, T. C.; Zwart, P. H. PHENIX: a comprehensive Python-based system for macromolecular structure solution. *Acta Crystallogr., Sect. D: Biol. Crystallogr.* **2010**, *66* (2), 213−221.
(44) Emsley, P.; Lohkamp, B.; Scott, W. G.; Cowtan, K. Features and development of Coot. *Acta Crystallogr., Sect. D: Biol. Crystallogr.* **2010**, *66* (4), 486−501.

https://dx.doi.org/10.1021/jacs.9b11699
J. Am. Chem. Soc. 2020, 142, 2386−2395

(45) Rose, A. S.; Bradley, A. R.; Valasatava, Y.; Duarte, J. M.; Prlić, A.; Rose, P. W. NGL viewer: web-based molecular graphics for large complexes. *Bioinformatics* **2018**, *34* (21), 3755−3758.
(46) Frisch, M. J.; Trucks, G. W.; Schlegel, H. B.; Scuseria, G. E.; Robb, M. A.; Cheeseman, J. R.; Scalmani, G.; Barone, V.; Petersson, G. A.; Nakatsuji, H.; Li, X.; Caricato, M.; Marenich, A. V.; Bloino, J.; Janesko, B. G.; Gomperts, R.; Mennucci, B.; Hratchian, H. P.; Ortiz, J. V.; Izmaylov, A. F.; Sonnenberg, J. L.; Williams-Young, D.; Ding, F.; Lipparini, F.; Egidi, F.; Goings, J.; Peng, B.; Petrone, A.; Henderson, T.; Ranasinghe, D.; Zakrzewski, V. G.; Gao, J.; Rega, N.; Zheng, G.; Liang, W.; Hada, M.; Ehara, M.; Toyota, K.; Fukuda, R.; Hasegawa, J.; Ishida, M.; Nakajima, T.; Honda, Y.; Kitao, O.; Nakai, H.; Vreven, T.; Throssell, K.; Montgomery, J. A.; Peralta, J. E.; Ogliaro, F.; Bearpark, M. J.; Heyd, J. J.; Brothers, E. N.; Kudin, K. N.; Staroverov, V. N.; Keith, T. A.; Kobayashi, R.; Normand, J.; Raghavachari, K.; Rendell, A. P.; Burant, J. C.; Iyengar, S. S.; Tomasi, J.; Cossi, M.; Millam, J. M.; Klene, M.; Adamo, C.; Cammi, R.; Ochterski, J. W.; Martin, R. L.; Morokuma, K.; Farkas, O.; Foresman, J. B.; Fox, D. J. *Gaussian 16*, Revision A.03; Gaussian, Inc.: Wallingford, CT, 2016.
(47) Glendening, E. D.; Badenhoop, J. K.; Reed, A. E.; Carpenter, J. E.; Bohmann, J. A.; Morales, C. M.; Landis, C. R.; Weinhold, F. *NBO 6.0*; Theoretical Chemistry Institute, University of Wisconsin: Madison, WI, 2012.

https://dx.doi.org/10.1021/jacs.9b11699
J. Am. Chem. Soc. 2020, 142, 2386−2395